A Unified Equation of State on a Microscopic Basis : Implications for Neutron Stars Structure and Cooling

IOP Conf. Series: Journal of Physics: Conf. Series **981** (2018) 012012 doi:10.1088/1742-6596/981/1/012012

A Unified Equation of State on a Microscopic Basis : Implications for Neutron Stars Structure and Cooling

G. F. Burgio

INFN Sezione di Catania, Via S. Sofia 64, I-95123 Catania, Italy

E-mail: fiorella.burgio@ct.infn.it

Abstract. We discuss the structure of Neutron Stars by modelling the homogeneous nuclear matter of the core by a suitable microscopic Equation of State, based on the Brueckner-Hartree-Fock many-body theory, and the crust, including the pasta phase, by the BCPM energy density functional which is based on the same Equation of State. This allows for a unified description of the Neutron Star matter over a wide density range. A comparison with other unified approaches is discussed. With the same Equation of State, which features strong direct Urca processes and using consistent nuclear pairing gaps as well as effective masses, we model neutron star cooling, in particular the current rapid cooldown of the neutron star Cas A. We find that several scenarios are possible to explain the features of Cas A, but only large and extended proton $^1S_0$ gaps and small neutron $^3PF_2$ gaps can accommodate also the major part of the complete current cooling data.

1. Introduction

In the past few years, the interplay between the observations and the theoretical predictions about neutron stars (NS) has stimulated an impressive progress in the field, and it is expected to help answering many fundamental questions on the properties of very dense matter and the corresponding elementary processes that can occur. Therefore it is necessary to construct models based on a sound theoretical background, in order to reduce the uncertainty on the possible conclusions one can draw from these studies.

The equation of state (EoS) of neutron-rich matter is a basic input needed to compute most properties of NS. A large amount of experimental data on nuclei, heavy ion collisions, and astrophysical observations has been used to constrain the nuclear EoS and, at the same time, to understand the structure and properties of NS [1]. Unfortunately, a direct link of measurements and observations with the underlying EoS is very difficult, and a big uncertainty does exist about a proper interpretation of the data. To reduce the uncertainty on these types of analyses, it is helpful to develop a unified theory of matter, which is able to describe on a microscopic level the complete structure of NS from the outer crust to the core. This is not a simple task, since the methods developed for homogeneous nuclear matter cannot be easily extended to nuclei and to the non-homogeneous matter present in NS crust. Recently [2, 3, 4], the BCPM (Barcelona-Catania-Paris-Madrid) nuclear energy density functional has been developed in order to describe finite nuclei. This functional has been obtained from the *ab initio* Brueckner-Hartree-Fock (BHF) calculations in nuclear matter within an approximation inspired by the Kohn-Sham formulation of density functional theory [5]. We employ the BHF EoS and the corresponding BCPM functional to describe the whole NS structure, and compare with the results obtained with the few other methods that describe the whole NS structure within a unified theoretical scheme. In this paper we limit the treatment to only nucleon degrees of freedom, neglecting the possibility of the appearance of exotic components like hyperons and quarks,

for which the uncertainty is too large to perform a fruitful comparison with other approaches.

The interpretation of the signals coming from the astrophysical observations on the processes and phenomena that occur in NS does not require just a reliable Equation of State, but also additional theoretical tools. One of the most important is the temperature-vs.-age cooling diagram, in which currently a few (~ 20) observed NS are located. NS cooling is over a vast domain of time ($10^{-10} - 10^5$ yrs) dominated by neutrino emission due to several microscopic processes [6]. The theoretical analysis of these reactions requires the knowledge of the relevant beta-stable nuclear EoS, along with the superfluid properties of the stellar matter, i.e., the gaps and critical temperatures in the different pairing channels. The observation of very rapid cooling of the supernova remnant Cas A, for which different analyses deduce a temperature decline of about 2 to 5 percent during the last ten years [7, 8, 9], has stimulated an intense theoretical activity. Several theoretical scenarios have been proposed to explain this observation, e.g. a fine-tuned small neutron 3PF2 (n3P2) gap [10, 11, 12], that generates strong cooling at the right moment due to the superfluid neutron pair breaking and formation (PBF) mechanism [13]; a strongly reduced thermal conductivity of the stellar matter that delays the heat propagation from the core to the crust to a time compatible with the age of Cas A [14]; a strong dissipation of the small-scale magnetic field in the crust which produces Joule heating [15]; a transition from a fully gapped two-flavor color-superconducting phase to a gapless/ crystalline phase [16]. A common feature of all these cooling scenarios is that EoS and pairing gaps are treated in disjoint and inconsistent manner, i.e., a given EoS is combined with pairing gaps obtained within a different theoretical approach and using different input interactions. Moreover all those approaches exclude from the beginning the possibility of very fast direct Urca (DU) cooling, although many microscopic nuclear EoS do reach easily the required proton fractions for this process [17, 18, 19]. In a recent paper [20] EoS and nuclear pairing gaps have been obtained with exactly the same nuclear (in-medium) interaction, as well as nucleon effective masses [21], which affect the neutrino emissivities. Moreover the DU cooling process as predicted by the BHF microscopic nuclear EOS have been consistently taken into account.

The present article is organized as follows. In Sect. II we present the models of the EOS considered in this work respectively for the NS crust and core, with a discussion of the results obtained for the NS structure. In Sect. III we analyze several possible cooling scenarios derived within our consistent approach, and discuss the results. Finally, our concluding remarks are drawn in Sect. IV.

2. EOS of nuclear matter

In this section we remind briefly the Brueckner-Hartree-Fock (BHF) method for the nuclear matter EOS [22, 1]. The main ingredient is the calculation of the in-medium G-matrix nucleon-nucleon (NN) interaction from the bare NN potential V,

$$G[\rho;\omega] = V + \sum_{k_a k_b} V \frac{|k_a k_b\rangle Q \langle k_a k_b|}{\omega - e(k_a) - e(k_b)} G[\rho;\omega]\,, \tag{1}$$

where $\rho = \sum_{k<k_F}$ is the nucleon number density, and ω the starting energy. The single-particle (s.p.) energy (assuming $\hbar = 1$)

$$e(k) = e(k;\rho) = \frac{k^2}{2m} + U(k;\rho) \tag{2}$$

and the Pauli operator Q determine the propagation of intermediate baryon pairs. The BHF approximation for the s.p. potential $U(k;\rho)$ using the *continuous choice* prescription is

$$U(k;\rho) = \mathrm{Re} \sum_{k'<k_F} \langle kk'|G[\rho; e(k) + e(k')]|kk'\rangle_a\,, \tag{3}$$

where the subscript a indicates antisymmetrization of the matrix element. Due to the occurrence of $U(k)$ in Eq. (2), these equations constitute a coupled system that has to be solved in a self-consistent manner

for several momenta of the particles involved, at the considered densities. In the BHF approximation the energy per nucleon is given by

$$\frac{E}{A} = \frac{3}{5}\frac{k_F^2}{2m} + \frac{1}{2\rho}\sum_{k,k' \leq k_F} \langle kk'|G[\rho; e(k) + e(k')]|kk'\rangle_a. \quad (4)$$

In this scheme, the only input quantity needed is the bare NN interaction V in the Bethe-Goldstone equation (1). In this work we use the Argonne V_{18} NN ipotential [23] as the two-nucleon interaction. The resulting nuclear EoS can be calculated with good accuracy in the Brueckner two hole-line approximation with the continuous choice for the single-particle potential, being the results in this scheme quite close to the calculations which include also the three hole-line contribution [24].

Since non-relativistic calculations, based on purely two-body interactions, fail to reproduce the correct saturation point of symmetric nuclear matter, the bare NN interaction has to be supplemented by a suitable three-nucleon force (TBF). For that, TBF are reduced to a density dependent two-body force by averaging over the generalized coordinates (position, spin and isospin) of the third particle, assuming that the probability of having two particles at a given distance is reduced according to the two-body correlation function [25, 26, 27]. In this work we will illustrate results obtained using a phenomenological approach to the TBF, which is based on the so-called Urbana model [28, 29]. Within the BHF approach, those TBF produce a shift of about +1 MeV in energy and -0.1 fm^{-3} in density, and is obtained by tuning the two parameters contained in the TBF in order to get an optimal saturation point [25, 26].

Besides a purely phenomenological model, microscopic TBF have also been derived and a tentative approach proposed using the same meson-exchange parameters as the underlying NN potential [30, 31]. However, at present the theoretical status of microscopically derived TBF is still quite rudimentary, Alternatively, latest nuclear matter calculations [32, 33] using chiral inspired TBF [34, 35], showed that the considered TBF models are not able to reproduce simultaneously the correct saturation point and the properties of three- and four-nucleon systems. Therefore, the role of TBF is still an important open question, but it may be greatly reduced if the NN potential is based on a realistic constituent quark model [36, 37] which can explain at the same time few-nucleon systems and nuclear matter, including the observational data on Neutron Stars and the experimental data on heavy-ions collisions.

In the past years, the BHF approach has been extended in order to include the hyperon degrees of freedom [38, 39], which are expected to appear in neutron star matter already at relatively low densities, thus producing a softening of the EoS with a strong decrease of the maximum mass. Accurate theoretical calculations of hypernuclear matter, starting from the available information on both nucleon and hyperon interactions, were performed in the past years. In the Brueckner scheme, we used the phenomenological nucleon-hyperon potentials [40, 41, 42] as fundamental input, while the hyperon-hyperon potentials were neglected due to the lack of appropriate experimental data. We found very low maximum masses of hyperon stars, below 1.4 $M_\odot$ ($M_\odot = 2 \times 10^{33}$g). Several proposals of this so-called *hyperon puzzle* have been put forward [43, 44, 45], but many inconsistencies still remain, and the solution to this problem is still far from being understood.

2.1. The crust region

A NS interior consists of three main regions, namely, an outer crust, an inner crust, and a core. The outer crust region [46] consists of matter composed by neutron-rich nuclei permeated by a degenerate electron gas, at densities approximately between 10^4 g/cm^3, where atoms become completely ionized, and 4×10^{11} g/cm^3, where neutrons start to drip from the nuclei. The nuclei arrange themselves in a solid body-centred cubic (bcc) lattice in order to minimize the Coulomb repulsion, and are stabilized against β decay by the surrounding electron gas. At the low densities of the beginning of the outer crust, the Coulomb lattice is populated by ^{56}Fe nuclei. As the density of matter increases with increasing depth in the crust, it becomes energetically favourable for the system to lower the proton fraction through electron captures with the energy excess carried away by neutrinos. The system progressively evolves towards

a lattice of more and more neutron-rich nuclei as it approaches the bottom of the outer crust, until the neutron drip density is reached and the inner crust of the NS begins.

The structure of the inner crust consists of a Coulomb lattice of nuclear clusters permeated by the gases of free electrons and neutrons, such that the whole system is charge neutral. The neutron fraction increases with growing matter density. At the bottom layers of the inner crust, the nuclear clusters may adopt non-spherical shapes in order to minimize their energy [47, 48, 49, 50], and the equilibrium nuclear shape may change from sphere, to cylinder, slab, tube (cylindrical hole), and bubble (spherical hole) before going into uniform matter. These shapes are generically known as "nuclear pasta".

The EoS derived in the BHF scheme was used to construct the BCPM (Barcelona-Catania-Paris-Madrid) nuclear energy density functional for describing finite nuclei, as explained in ref. [2]. The BCPM functional is built up with a bulk part obtained directly from the BHF results in symmetric and neutron matter via the local density approximation. Additional ingredients of the functional are a phenomenological surface energy term, necessary to describe correctly the nuclear surface, together with the Coulomb, spin-orbit, and a pairing contribution to describe open-shell nuclei. The resulting functional has only four open parameters, which have been determined by minimizing the root-mean-square (rms) deviation σ_E between the theoretical and experimental binding energies of a set of well-deformed nuclei in the rare-earth, actinide, and super-heavy mass regions of the nuclear chart [3]. The predictive power of the functional is then tested by computing the binding energies of 467 known spherical nuclei. A fairly reasonable rms deviation $\sigma_E = 1.3$ MeV between theory and experiment is found. This gives confidence to the use of this functional for the study of the NS crust, where very asymmetric nuclei appear. In particular, the EoS of the outer crust requires the masses of neutron-rich nuclei, and those are obtained through Hartree-Fock-Bogoliubov calculations with the BCPM functional when they are unknown experimentally. To compute the inner crust, Thomas-Fermi (TF) calculations in Wigner-Seitz cells are performed with the same BCPM functional. Different shapes of the elementary cells of the lattice are tested in order to determine the most favourable structure. Existence of nuclear pasta is predicted in a range of average baryon densities between $\simeq 0.067$ fm^{-3} and $\simeq 0.0825$ fm^{-3}, where the transition to the core takes place. More details on the BCPM functional can be found in ref. [2].

2.2. The high-density EOS

The core is the internal region at densities larger than 1.5×10^{14} g/cm^3, where matter forms a homogeneous liquid composed of neutrons plus a certain fraction of protons, electrons, and muons that maintain the system in β equilibrium. Deep in the core, at still higher densities, strange baryons and even deconfined quarks may appear [51, 52]. In the center of a NS the baryon density can reach values that are several times larger than the nuclear saturation density. The core includes most of the NS mass and therefore the high-density EoS is crucial. We adopt a conventional description of the core as being composed by homogeneous asymmetric nuclear matter and a gas of electrons and muons. The EoS for the liquid core is derived in the framework of the BHF theory just described.

In order to study the structure of the NS core, we have to calculate the composition and the EoS of cold, neutrino-free, catalyzed matter in the following standard way. The Brueckner calculation yields the energy density of lepton/baryon matter as a function of the different partial densities,

$$\begin{aligned}\varepsilon(n_n,n_p,n_e,n_\mu) &= (n_n m_n + n_p m_p) + (n_n+n_p)\frac{E}{A}(n_n,n_p)\\ &+ \varepsilon(n_\mu)+\varepsilon(n_e)\,,\end{aligned} \tag{5}$$

where we have used ultrarelativistic and relativistic approximations for the energy densities of electrons and muons, respectively. In practice, it is sufficient to compute only the binding energy of symmetric nuclear matter and pure neutron matter, since within the BHF approach it has been verified [53, 54, 55] that a parabolic approximation for the binding energy of nuclear matter with arbitrary proton fraction

$x_p = n_p/n_b$, $n_b = n_n + n_p$, is well fulfilled,

$$\frac{E}{A}(n_b, x_p) \approx \frac{E}{A}(n_b, x_p = 0.5) + (1 - 2x_p)^2 E_{\rm sym}(n_b)\,, \tag{6}$$

where the symmetry energy $E_{\rm sym}$ can be expressed in terms of the difference of the energy per particle between pure neutron ($x_p = 0$) and symmetric ($x_p = 0.5$) matter:

$$E_{\rm sym}(n_b) = -\frac{1}{4}\frac{\partial(E/A)}{\partial x_p}(n_b, 0) \approx \frac{E}{A}(n_b, 0) - \frac{E}{A}(n_b, 0.5)\,. \tag{7}$$

Knowing the energy density Eq. (5), the various chemical potentials (of the species $i = n, p, e, \mu$) can be computed straightforwardly,

$$\mu_i = \frac{\partial \varepsilon}{\partial n_i}\,, \tag{8}$$

and the equations for beta-equilibrium,

$$\mu_i = b_i \mu_n - q_i \mu_e\,, \tag{9}$$

(b_i and q_i denoting baryon number and charge of species i) and charge neutrality,

$$\sum_i n_i q_i = 0\,, \tag{10}$$

allow one to determine the equilibrium composition n_i at given baryon density n_b and finally the EoS,

$$P(n_b) = n_b^2 \frac{d}{dn_b}\left(\frac{\varepsilon(n_i(n_b))}{n_b}\right) = n_b \frac{d\varepsilon}{dn_b} - \varepsilon = n_b \mu_n - \varepsilon\,. \tag{11}$$

2.3. Results and Discussion

In this Section, we will report on the main results obtained for the EoS, and compare with the few nuclear EoS that have been devised and used to cover the whole NS structure.

A partly phenomenological approach, based on the compressible liquid drop model, has been developed by Lattimer and Swesty (LS) [56]. It can cover the whole range of density, including the crust and the pasta phase, and it gives a complete description of the NS matter structure. This EoS is derived from a macroscopic functional, and it is compatible with an accurate mass formula throughout the nuclear table. There are different versions of this EoS, and here we present results obtained with the SKa version, which is characterized by an incompressibility $K = 264$ MeV.

Another approach with similar characteristics has been developed by Shen et al. (SH) [57, 58], and it is based on a nuclear relativistic mean field (RMF) model. The crust was described in the Thomas-Fermi scheme using the variational method with trial profiles for the nucleon densities. For the SH EoS the incompressibility is $K = 281$ MeV. The LS and SH EoS are widely used in astrophysical calculations for both neutron stars and supernova simulations due to their numerical simplicity and the large range of tabulated densities and temperatures.

Other approaches employ Skyrme forces to calculate the whole structure of NS. In ref. [59] the force SLy4 was used, and since this force was adjusted to reproduce the pure neutron matter EOS of Friedman and Pandharipande [60], this approach contains some microscopic input. In this case the incompressibility is about $K = 230$ MeV. This EoS is also known as the Douchin-Haensel EoS. More recently a similar approach was followed in refs. [61, 62], where the Skyrme forces BSk19, BSk20 and BSk21 were used, each one adjusted to a different microscopic neutron matter EOS with different stiffness at high density. Analytical fits of these neutron star EoS have been constructed in order to facilitate their inclusion in

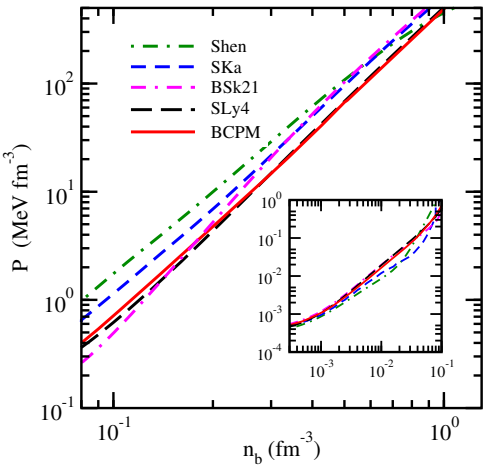

Figure 1. (Color online) The pressure P is displayed vs. the baryon density for several EoS. In the inset the inner crust EoS is plotted. See text for details.

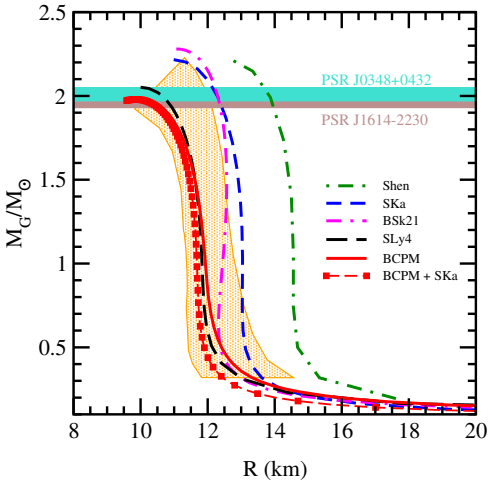

Figure 2. (Color online) The gravitational mass M_G is plotted vs. the radius R for the cases displayed in Fig.1.

astrophysical simulations [63]. Here we consider the BSk21 version of that EoS as a representative example, being characterized by an incompressibility $K = 246$ MeV.

In Fig. 1 we compare the EoS derived from the BHF theory and the BCPM functional (solid red) with the just mentioned EoS. The density range extends from the crust-core density, located around $0.08\,\mathrm{fm}^{-3}$, up to typical NS core densities. We notice a remarkable similarity with the SLy4 EoS (long-dashed, black), whereas a strong difference with the SKa EoS (short-dashed, blue), the SH EoS (dot-dashed, green), and the BSk21 EoS (dot-dashed-dashed, magenta) is observed. In the inset we report the EoS of the inner crust starting from neutron drip $\mathrm{n_{drip}} = 3 \times 10^{-4}\,\mathrm{fm}^{-3}$. We observe that the pressures from the Lattimer-Swesty EoS and the Shen EoS differ significantly from BCPM and SLy4 EoS. However, the BCPM and SLy4 pressures in the inner crust show an impressive concordance with BSk21 that remains within the core region up to about 0.2 fm^{-3}, but is not maintained in the extrapolation to higher densities, where the BSk21 and Lattimer-Swesty models predict the stiffest EoS. We recall that, despite the crust contains a small fraction of the NS mass, its EoS and its matching with the core EoS can be relevant for the determination of the NS radius. Once the EoS of nuclear matter is known, one can use the well-known Tolman-Oppenheimer-Volkoff equations for spherically symmetric NS:

$$\begin{aligned} \frac{dP}{dr} &= -G\frac{\varepsilon m}{r^2}\left(1+\frac{P}{\varepsilon}\right)\left(1+\frac{4\pi P r^3}{m}\right)\left(1-\frac{2Gm}{r}\right)^{-1} \\ \frac{dm}{dr} &= 4\pi r^2 \varepsilon\,, \end{aligned} \tag{12}$$

where G is the gravitational constant, P the pressure, ε the energy density, m the mass enclosed within a radius r, and r the (relativistic) radius coordinate. To close the equations we need the relation between pressure and density, $P = P(\varepsilon)$, i.e. just the EoS. Integrating these equations one gets the mass and radius of the star for a given central density. As shown in Fig.2, the considered EoS are compatible with the largest mass observed up to now, which is close to $2.01 \pm 0.04\,M_\odot$ in PSR J0348+0432 [64], and displayed in Fig.2, along with the previously observed mass of PSR J1614-2230 [65] having $M_G = 1.97 \pm 0.04\,M_\odot$. For completeness, we also display in the orange hatched band the probability distribution for $\mathrm{M_G}$ and R deduced from five PRE (Photospheric Radius Expansion) burst sources and five QLMXB sources, after a Bayesian analysis [66]. We see that, except the Shen EoS, all EoS are compatible with the observational

data. Moreover we find that the mass-radius relationship calculated with SLy4 EoS is surprisingly close to the one obtained with BHF EoS and the consistent BCPM functional for the crust, which can be explained by the close value of the respective bulk incompressibility. We also notice that the maximum mass calculated with the BCPM and the SLy4 EoS is characterized by a radius of about 10 km, which is somewhat smaller than the radius calculated with the other considered EoS, in line with recent analyses of observations on quiescent low-mass X-ray binaries (QLMXB) [67] and X-ray bursters [68], for which more studies could however be needed [69]. In order to study the role of the crust for the values of the NS radius, we have performed calculations using the BHF EoS for the core and the LS-SKa EoS for the crust. The results are reported in the same Fig. 2 (red squares). One can see that the use of LS-SKa crust EOS makes only a relatively small effect on the mass-radius relationship, being most relevant for masses smaller than $1\,M_\odot$, where the crust has a prominent relevance. This shows the importance of using the EoS derived from the same theoretical scheme both for the crust and the core. In fact, matching the core EoS with a crust EoS from a different model can introduce uncertainties for the NS structure.

3. Neutron star cooling simulations

A unified description of the EoS turns out to be very important also in the NS cooling simulations. We recall that the main cooling regulators are the neutrino emissivities and the nuclear pairing gaps. In most of the cooling simulations, the EoS and pairing gaps are treated in a disjoint and inconsistent way, i.e. they are obtained using different NN in-medium interaction. Recently a tentative step towards a consistent description has been performed [20].

We remind that in a non-superfluid scenario three main mechanisms of neutrino emission are usually taken into account, which are the direct Urca (DU), the modified Urca (MU), and the NN bremsstrahlung (BNN) processes. By far the most efficient mechanism of NS cooling is the DU process, for which the derivation of the neutrino emissivity Q under the condition of β equilibrium gives

$$Q^{(DU)} \approx 4.0 \times 10^{27} \left(\frac{\rho_p}{\rho_0}\right)^{1/3} \left(\frac{m_n^*}{m_n}\right) \left(\frac{m_p^*}{m_p}\right) T_9^6\, \Theta(k_{F_p} + k_{F_e} - k_{F_n})\,, \tag{13}$$

where T_9 is the temperature in units of 10^9K, and the emissivity $Q^{(DU)}$ is given in units of erg cm^{-3} s^{-1}. If muons are present, then the corresponding DU process may also become possible, in which case the neutrino emissivity is increased by a factor of 2. In Eq.(13) ρ_p is the proton population, which depends on the behaviour of the symmetry energy, while m_n^*, m_p^* are the neutron and proton effective masses. In the BHF approach they are easily calculated as

$$\frac{m^*(k)}{m} = \frac{k}{m}\left[\frac{de(k)}{dk}\right]^{-1}, \tag{14}$$

i.e. they are derived consistently from the BHF single-particle energy $e(k)$, Eq. (2), [21]. Although the effect is not large compared to other uncertainties, such a consistent treatment is hard to find in previous works. We recall that the BHF EoS predicts a density onset value for DU process close to $\rho = 0.44\,\mathrm{fm}^{-3}$, and therefore with our EoS fast cooling is active in nearly all stars with $M/M_\odot > 1.10$. This is at variance with the APR EoS [70], widely used in cooling simulations, where the DU process is delayed to $\rho = 0.82\,\mathrm{fm}^{-3}$, and therefore it is active only in the heaviest stars, $M/M_\odot > 2.03$. This has strong consequences for the cooling behaviour.

Of vital importance for any cooling simulation is the knowledge of the 1S0 and 3PF2 pairing gaps for neutrons and protons in beta-stable matter, which on one hand block the DU and MU reactions, and on the other hand open new cooling channels by the pair breaking and formation (PBF) mechanism for stellar matter in the vicinity of the critical temperature [6]. In this work we focus on the most important proton 1S0 (p1S0) and neutron 3PF2 (n3P2) pairing channels. As already stressed, the gaps should be computed in a framework that is consistent with the determination of the EOS, i.e., be based on the same

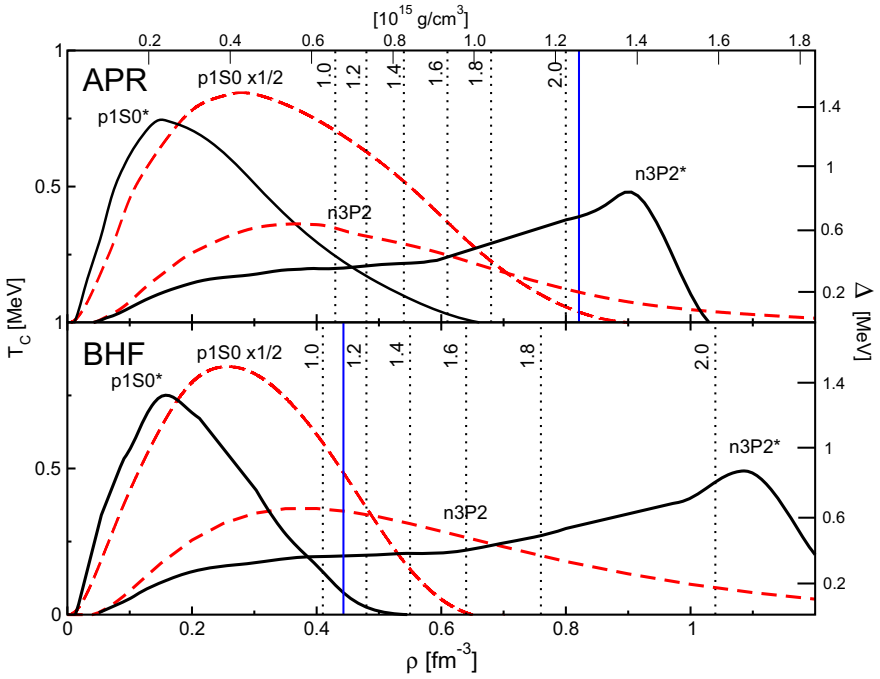

Figure 3. (Color online) Pairing gaps in NS matter in the p1S0 and n3P2 channels, including (*) or not effective mass effects. In the upper (lower) panel results are displayed for the APR(BHF) EoS. Vertical dotted lines indicate the central density of NS with different masses $M/M_\odot = 1.0, \ldots, 2.0$. DU onset occurs at the vertical solid (blue) lines.

NN interaction and using the same medium effects (TBF and effective masses). Indeed in ref. [71] the same Argonne V_{18} + UIX Urbana nuclear interaction and BHF s.p. spectra were employed for the calculation of the gaps by solving the (angle-averaged) gap equation on the BCS level [72, 73, 74, 75, 76].

Fig. 3 displays the p1S0 and n3P2 pairing gaps as a function of baryonic density of beta-stable matter for the APR (upper panel) and the fully consistent BHF (lower panel) EoS models. Pairing gaps calculated with only the two-body force V_{18} together with the kinetic s.p. energies are represented by dashed-red curves, whereas curves denoted by p1S0* and n3P2* are obtained using the BHF s.p. spectra. Since polarization corrections are uncertain [77, 78, 79], we use scaling factors for the proton and neutron gaps, s_p and s_n, respectively. Qualitatively one observes in Fig. 3 the natural scaling effect of the different proton fractions for the BHF and APR EoS, such that the p1S0 gaps extend to larger (central) densities for the APR model, due to the lower proton fraction in that case. Therefore the blocking effect on the cooling extends up to higher densities and NS masses for the APR model. In both cases, the n3P2$^{(*)}$ gaps extend up to very large density and can thus provide an efficient means to block this cooling process, in particular for the n3P2* model comprising medium effects. The price to pay is an enhanced PBF cooling rate close to the critical temperature in that case.

A further important ingredient of the cooling simulations is the (leptonic and baryonic) thermal conductivity [6]. Recently it has been conjectured [14, 80, 81, 82] that the conductivities could be substantially suppressed by in-medium effects, and this could explain the rapid Cas A cooling. Hence we introduce a further scale factor s_κ for the total thermal conductivity. In the next subsection we present some results for certain choices of the three global parameters, i.e. s_p, s_n, s_κ.

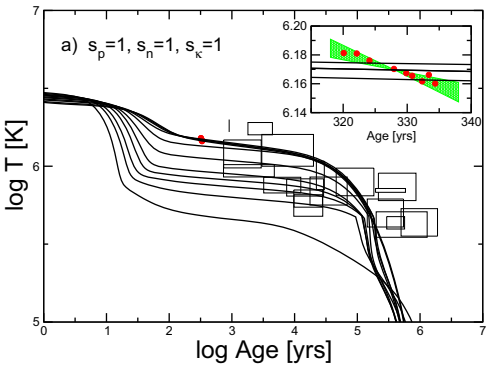

Figure 4. (Color online) Cooling curves without scaling factors for different NS masses $M/M_\odot = 1.0, 1.1, \ldots, 2.0$. BCS gaps with free s.p. spectra are employed. Red dots show the Cas A cooling data (enlarged in the inset).

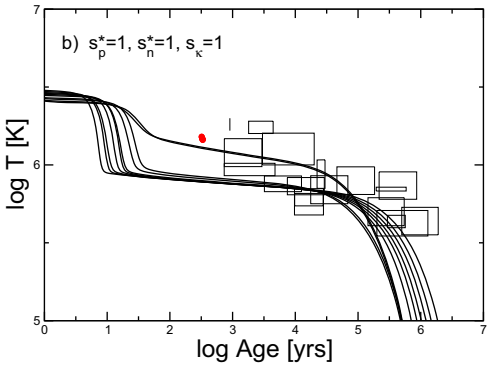

Figure 5. (Color online) Same as Fig.4, but BCS gaps are calculated with the BHF s.p. spectra.

3.1. Neutron star cooling and Cas A

We carried out the NS cooling simulations employing the widely used code `NSCool` [83], and including in our set of observational cooling data the (age, temperature) information of the 19 isolated NS sources listed in [84].

We begin by showing the results obtained with the original pairing gaps shown in Fig. 3, and without any modification of the conductivities, i.e., putting $s_p = s_n = s_k = 1$. Only the BHF EoS was used. Fig. 4 shows the temperature vs age results (11 curves for NS with masses $1.0, 1.1, \ldots, 2.0$) obtained with the BCS gaps without any medium modification (dashed red curves in the lower panel of Fig. 3), while Fig. 5 employs the BCS gaps with BHF effective masses (black curves in Fig. 3), and is indicated by the notation $s_p^* = s_n^* = 1$ here and in the following. One observes results in line with the features of the pairing gaps, namely in Fig. 4 light ($M < 1.4\,M_\odot$) NS cool slower and heavy ($M > 1.7\,M_\odot$) NS cool faster than in Fig. 5. This is due to the larger overall values of the corresponding BCS gaps in the low-density ($n < 0.6\,\mathrm{fm}^{-3}$) region and the smaller n3P2 value in the high-density ($n > 0.7\,\mathrm{fm}^{-3}$) domain, see Fig. 3, which cause, respectively, a stronger or weaker blocking of the dominant DU process in light or heavy stars. In both scenarios, it is possible to explain cold stars due to the DU mechanism in the BHF model, but they cannot reproduce the particular cooling properties of Cas A: While the first one can fit its current age and temperature as a $M = 1.2\,M_\odot$ NS, neither reproduces the apparent very fast current cooldown [7, 8, 9] shown in the inset of Fig. 4.

Alternative scenarios have been proposed, e.g. one based on an appropriately chosen n3P2 gap, which causes strong cooling due to the opening of the neutron PBF process at the current age/temperature of the star. The BHF EOS including strong DU reactions also allows this interpretation by choosing the scaling factors $s_p = 2.0$, $s_n = 0.132$, $s_\kappa = 1$ for a $1.4\,M_\odot$ star, corresponding to maximum values of the gaps $\Delta_p \approx 6\,\mathrm{MeV}$ and $\Delta_n \approx 0.1\,\mathrm{MeV}$, i.e., Δ_p is larger than usually chosen while Δ_n is in line with the equivalent results of [85, 10, 11, 12]. The results are shown in Fig. 6, which displays the sequence of cooling curves for NS masses $M/M_\odot = 1.0, 1.1, \ldots, 2.0$, the 1.4 case corresponding to Cas A by construction. In this case the neutron $^1S_0$ gap has been rescaled by a factor 0.04 for fine tuning.

As in similar investigations [13, 85], one notes that the rapid cooldown caused by the n3P2 PBF renders even more difficult the reproduction of very old and warm stars, which are not covered by any cooling curve. As already mentioned, a possible alternative scenario predicts a strong suppression of the lepton and baryon thermal conductivities due to in-medium effects [14, 82]. The reduced conductivity serves to

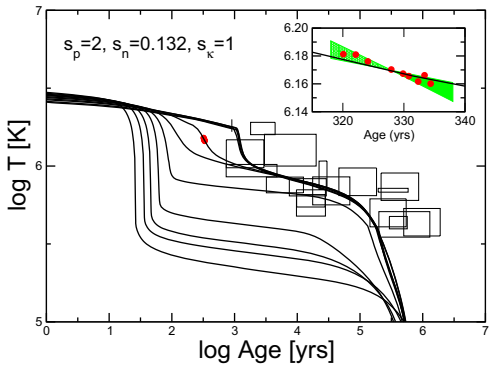

Figure 6. (Color online) Same as Fig. 4, but for the PBF cooling scenario. The M = $1.4\,M_\odot$ cooling curve passes through Cas A by construction.

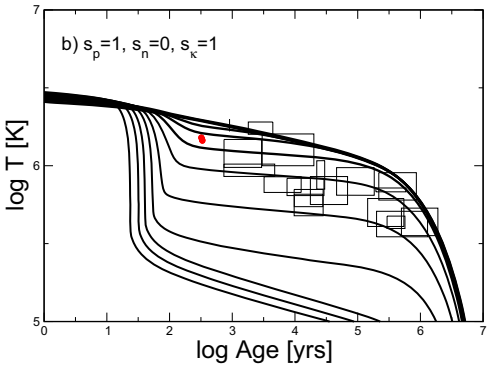

Figure 7. Same as Fig. 4, using $s_p = 1$, $s_n = 0$ and $s_k = 1$.

delay the temperature decline up to the current age of Cas A without need to introduce fine-tuned nPBF cooling. Our EoS including DU cooling also accommodates this possibility, and a rather satisfactory fit of all cooling data including Cas A, is obtained employing the parameter set $s_p^* = 1$, $s_n^* = 0$, $s_\kappa = 0.135$, where the size of s_κ is comparable to the values of about 0.2 deduced in [14, 82]. In this scenario a rather small value of the n3P2 gap seems to be required, as otherwise old hot (and also young cold) NS cannot be obtained, even if Cas A is reproduced. More details are reported in ref.[20].

The previous results have demonstrated that it is difficult to satisfy simultaneously the slow cooling of old NS and the rapid cooling of Cas A, in which case some doubts have been expressed about the validity of the data analysis [86], and a future revision towards much slower or no cooling at all is not excluded.

We therefore study finally a scenario without the Cas A constraint (apart from reproducing its current age and temperature with a reasonable mass) in our strong DU model, trying to cover the full range of current cooling data. Considering that the use of the unscaled BCS gaps in Fig. 4 yields already a reasonable reproduction of most young NS, and considering the fact that a finite n3P2 gap produces too strong PBF cooling, simply switching off this channel yields a nearly perfect coverage of all current cooling data, as shown in Fig. 7. In this scenario Cas A turns out to be a $1.31\,M_\odot$ NS. Thus the BCS p1S0 gap alone is able to suppress sufficiently the DU cooling, provided that it extends over a large enough density range. Though in our case the p1S0 gap is perhaps somewhat large, we have investigated the effect of its rescaling, finding excellent cooling simulations, with the predicted mass of Cas A being between $1.18\,M_\odot$ and $1.46\,M_\odot$. Therefore a precise information on the masses of the NS in the cooling diagram is necessary, without which no theoretical cooling model can be verified.

4. Conclusions

We have presented a study of NS structure by focusing on microscopic models which are able to describe on the same theoretical framework both the core and the crust regions. To this purpose we have performed calculations of NS structure based on the EoS derived within the Brueckner-Hartree-Fock scheme. This EoS is the basis of the BCPM, a recent and accurate nuclear energy density functional [2] devised to reproduce nuclear binding energies throughout the nuclear mass table and, as such, used also to calculate the structure of NS crust. The resulting EoS has been used to calculate the overall NS structure, from the crust to the core, and the results compared with other more phenomenological models that also are able to describe the whole NS structure. In particular, we have chosen the Lattimer-Swesty [56], Shen [57, 58], BSk21 [61, 62], and the Douchin-Haensel EoS [59]. The role of the NS crust EoS has been emphasized as far as the radius for for the lightest NS masses is concerning. This indicates the relevance

of using models that are based on the same physical framework both for the crust and the core.

Following the same point of view, we have studied NS cooling using the microscopic BHF EoS, which features strong DU reactions already for $M/M_{\odot} > 1.10$, and using compatible p1S0 and n3P2 pairing gaps as well as nucleon effective masses. The current substantial theoretical uncertainty regarding gaps and thermal conductivity was modelled in a rather simple way by introducing three global scale factors. We have found that it is possible to reproduce the apparent fast cooling of Cas A by either fine tuning the n3P2 pairing gap or reducing the thermal conductivity. In general it is difficult to fit simultaneously the rapid cooling of Cas A and old and warm NS, but once the Cas A constraint is relaxed, all current cooling data can be fit by just assuming the p1S0 BCS gap and a vanishing n3P2 gap.

In summary, it is very difficult to draw quantitative conclusions from the current NS cooling data on the properties of matter at large densities if the masses of the cooling objects are unknown, due to the large variety of required microphysics input.

Acknowledgments
We acknowledge useful discussions with M. Baldo, H.-J. Schulze, X. Viñas and W. Ho. Partial support comes from "NewCompStar," COST Action MP1304.

5. References

[1] Baldo M and Burgio G F 2012 *Rep. Prog. Phys.* **75** 026301
[2] Baldo M, Robledo L M, Schuck P and Viñas X 2013 *Phys. Rev. C* **87** 064305
[3] Baldo M, Schuck P and Viñas X 2008 *Physics Letters B* **663** 390–394
[4] Baldo M, Robledo L, Schuck P and Viñas X 2010 *Journal of Physics G Nuclear Physics* **37** 064015
[5] Kohn W and Sham L J 1965 *Physical Review* **140** 1133–1138
[6] Yakovlev D G, Kaminker A D, Gnedin O Y and Haensel P 2001 *Phys. Rep.* **354** 1–155
[7] Ho W C G and Heinke C O 2009 *Nature* **462** 71–73
[8] Heinke C O and Ho W C G 2010 *Astrophys. J. Lett.* **719** L167–L171
[9] Elshamouty K G, Heinke C O, Sivakoff G R, Ho W C G, Shternin P S, Yakovlev D G, Patnaude D J and David L 2013 *Astrophys. J.* **777** 22
[10] Page D, Prakash M, Lattimer J M and Steiner A W 2011 *Phys. Rev. Lett.* **106** 081101
[11] Yakovlev D G, Ho W C G, Shternin P S, Heinke C O and Potekhin A Y 2011 *Mon. Not. R. Astron. Soc.* **411** 1977–1988
[12] Shternin P S, Yakovlev D G, Heinke C O, Ho W C G and Patnaude D J 2011 *Mon. Not. R. Astron. Soc.* **412** L108–L112
[13] Page D, Lattimer J M, Prakash M and Steiner A W 2009 *Astrophys. J.* **707** 1131–1140
[14] Blaschke D, Grigorian H, Voskresensky D N and Weber F 2012 *Phys. Rev. C* **85** 022802
[15] Bonanno A, Baldo M, Burgio G F and Urpin V 2014 *Astron. Astrophys.* **561** L5
[16] Sedrakian A 2013 *Astron. Astrophys.* **555** L10
[17] Li Z H and Schulze H J 2008 *Phys. Rev. C* **78** 028801
[18] Burgio G F and Schulze H J 2010 *Astron. Astrophys.* **518** A17
[19] Taranto G, Baldo M and Burgio G 2013 *Phys. Rev. C* **87** 045803
[20] Taranto G, Burgio G F and Schulze H J 2016 *Mon. Not. R. Astron. Soc.* **456** 1451–1458
[21] Baldo M, Burgio G F, Schulze H J and Taranto G 2014 *Phys. Rev. C* **89** 048801
[22] Baldo M (ed) 1999 *Nuclear Methods and The Nuclear Equation of State* (Singapore: World Scientific)
[23] Wiringa R B, Stoks V and Schiavilla R 1995 *Phys. Rev. C* **51** 38–51
[24] Song H, Baldo M, Giansiracusa G and Lombardo U 1998 *Phys. Rev. Lett.* **81** 1584–1587
[25] Baldo M, Bombaci I and Burgio G 1997 *Astron.Astrophys.* **328** 274–282
[26] Zhou X R, Burgio G F, Lombardo U, Schulze H J and Zuo W 2004 *Phys. Rev. C* **69** 018801
[27] Lovato A, Benhar O, Fantoni S, Illarionov A Y and Schmidt K E 2011 *Phys. Rev.* **C83** 054003
[28] Carlson J, Pandharipande V and Wiringa R B 1983 *Nucl. Phys. A* **401** 59–85
[29] Schiavilla R, Pandharipande V and Wiringa R B 1986 *Nucl. Phys. A* **449** 219–242
[30] Li Z, Lombardo U, Schulze H J and Zuo W 2008 *Phys. Rev. C* **77** 034316
[31] Li Z and Schulze H 2012 *Phys. Rev. C* **85** 064002
[32] Lovato A, Benhar O, Fantoni S and Schmidt K E 2012 *Phys. Rev. C* **85** 024003
[33] Logoteta D, Vidaña I, Bombaci I and Kievsky A 2015 *Phys. Rev. C* **91** 064001
[34] Coon S A and Han H K 2001 *Few-Body Systems* **30** 131–141
[35] Navrátil P 2007 *Few-Body Systems* **41** 117–140
[36] Baldo M and Fukukawa K 2014 *Phys. Rev. Lett.* **113** 242501
[37] Fukukawa K, Baldo M, Burgio G F, Lo Monaco L and Schulze H J 2015 *Phys. Rev. C* **92** 065802

[38] Baldo M, Burgio G F and Schulze H 1998 *Phys. Rev. C* **58** 3688–3695
[39] Baldo M, Burgio G and Schulze H 2000 *Phys. Rev. C* **61** 055801
[40] Maessen P M M, Rijken T A and de Swart J J 1989 *Phys. Rev. C* **40** 2226–2245
[41] Stoks V G J and Rijken T A 1999 *Phys. Rev. C* **59** 3009–3020
[42] Schulze H J and Rijken T 2011 *Phys. Rev.* **C84** 035801
[43] Lonardoni D, Pederiva F and Gandolfi S 2014 *Phys. Rev. C* **89** 014314
[44] Vidaña I, Logoteta D, Providencia C, Polls A and Bombaci I 2011 *Europhys. Lett.* **94** 11002
[45] Yamamoto Y, Furumoto T, Yasutake N and Rijken T A 2014 *Phys. Rev. C* **90** 045805
[46] Baym G, Pethick C and Sutherland P 1971 *Astrophys. J.* **170** 299
[47] Baym G, Bethe H A and Pethick C J 1971 *Nuclear Physics A* **175** 225–271
[48] Ravenhall D G, Pethick C J and Wilson J R 1983 *Phys. Rev. Lett.* **50**(26) 2066–2069
[49] Lorenz C P, Ravenhall D G and Pethick C J 1993 *Phys. Rev. Lett.* **70**(4) 379–382
[50] Oyamatsu K 1993 *Nuclear Physics A* **561** 431–452
[51] Shapiro S L and Teukolsky S A 1983 *Black holes, white dwarfs, and neutron stars: The physics of compact objects* (New York: Wiley-Interscience)
[52] Haensel P, Potekhin A Y and Yakovlev D G 2006 *Neutron Stars 1: Equation of State and Structure* (New York: Springer)
[53] Bombaci I and Lombardo U 1991 *Phys. Rev. C* **44** 1892–1900
[54] Baldo M, Bombaci I and Burgio G F 1997 *Astron. Astrophys.* **328** 274–282
[55] Baldo M, Burgio G F and Schulze H J 2000 *Phys. Rev. C* **61** 055801
[56] Lattimer J M and Swesty D F 1991 *Nuclear Physics A* **535** 331–376
[57] Shen H, Toki H, Oyamatsu K and Sumiyoshi K 1998 *Progress of Theoretical Physics* **100** 1013–1031
[58] Shen H, Toki H, Oyamatsu K and Sumiyoshi K 1998 *Nucl. Phys. A* **637** 435–450
[59] Douchin F and Haensel P 2001 *Astron. Astrophys.* **380** 151–167
[60] Friedman B and Pandharipande V R 1981 *Nucl. Phys. A* **361** 502–520
[61] Pearson J M, Chamel N, Goriely S and Ducoin C 2012 *Phys. Rev. C* **85** 065803
[62] Fantina A F, Chamel N, Pearson J M and Goriely S 2013 *Astron. Astrophys.* **559** A128
[63] Potekhin A Y, Fantina A F, Chamel N, Pearson J M and Goriely S 2013 *Astron. Astrophys.* **560** A48
[64] Antoniadis J, Freire P, Wex N, Tauris T, Lynch R and et al 2013 *Science* **340** 1233232
[65] Demorest P B, Pennucci T, Ransom S M, Roberts M S E and Hessels J W T 2010 *Nature* **467** 1081–1083
[66] Lattimer J M and Steiner A W 2014 *European Physical Journal A* **50** 40
[67] Guillot S and Rutledge R E 2014 *Astrophys. J. Lett.* **796** L3
[68] Güver T and Özel F 2013 *Astrophys. J. Lett.* **765** L1
[69] Lattimer J M and Steiner A W 2014 *Astrophys. J.* **784** 123
[70] Akmal A, Pandharipande V R and Ravenhall D G 1998 *Phys. Rev. C* **58** 1804–1828
[71] Zhou X R, Schulze H J, Zhao E G, Pan F and Draayer J P 2004 *Phys. Rev. C* **70** 048802
[72] Amundsen L and Østgaard E 1985 *Nucl. Phys. A* **442** 163–188
[73] Baldo M, Cugnon J, Lejeune A and Lombardo U 1992 *Nucl. Phys. A* **536** 349–365
[74] Elgarøy Ø, Engvik L, Hjorth-Jensen M and Osnes E 1996 *Nucl. Phys. A* **607** 425–441
[75] Khodel V A, Khodel V V and Clark J W 1998 *Phys. Rev. Lett.* **81** 3828–3831
[76] Baldo M, Elgarøy Ø, Engvik L, Hjorth-Jensen M and Schulze H J 1998 *Phys. Rev. C* **58** 1921–1928
[77] Lombardo U and Schulze H J 2001 Superfluidity in Neutron Star Matter *Physics of Neutron Star Interiors* (*Lecture Notes in Physics, Berlin Springer Verlag* vol 578) ed Blaschke D, Glendenning N K and Sedrakian A p 30
[78] Sedrakian A and Clark J W 2006 *Nuclear Superconductivity in Compact Stars: BCS Theory and Beyond* (World Scientific Publishing Co) p 135
[79] Baldo M and Schulze H J 2007 *Phys. Rev. C* **75** 025802
[80] Shternin P S and Yakovlev D G 2007 *Phys. Rev. D* **75** 103004
[81] Shternin P S and Yakovlev D G 2008 *Astron. Lett.* **34** 675–685
[82] Blaschke D, Grigorian H and Voskresensky D N 2013 *Phys. Rev. C* **88** 065805
[83] Page D 2010 Nscool code available at http://www.astroscu.unam.mx/neutrones/nscool
[84] Beznogov M V and Yakovlev D G 2015 *Mon. Not. R. Astron. Soc.* **447** 1598–1609
[85] Ho W C G, Elshamouty K G, Heinke C O and Potekhin A Y 2015 *Phys. Rev. C* **91** 015806
[86] Posselt B, Pavlov G G, Suleimanov V and Kargaltsev O 2013 *Astrophys. J.* **779** 186